Electron-impact excitation heating rates in the atmosphere of Titan

L. Campbell,[1] H. Kato,[2] M. J. Brunger,[1] and M. D. Bradshaw[3]

Received 21 March 2010; revised 31 May 2010; accepted 28 June 2010; published 24 September 2010.

[1] A previous study of various heating rates in the atmosphere of Titan included electron-impact excitation of molecular nitrogen as one component. This work examines this component in more detail, using a statistical equilibrium calculation to avoid approximations made in the earlier work. The sensitivity of the results to different cross-section sets is investigated. It is found that using recent and more physical cross sections for vibrational excitation produces a significant increase in the heating rate. On the other hand, using more accurate cross sections for the electronic states had little apparent effect on the heating rates when used within the approximations made in the previous model. However, the inclusion of more transitions in this study produces a significant increase in the electronic state heating rates, as states that were originally neglected are now accounted for here.

Citation: Campbell, L., H. Kato, M. J. Brunger, and M. D. Bradshaw (2010), Electron-impact excitation heating rates in the atmosphere of Titan, *J. Geophys. Res.*, *115*, A09320, doi:10.1029/2010JA015482.

1. Introduction

[2] In a previous study of the atmosphere of Titan, *De La Haye et al.* [2008a] calculated heating rates produced by solar photons and by energetic electrons from Saturn's magnetosphere, via processes including the excitation of atmospheric molecules by electron impact, suprathermal electron heating, and the energy release through ion and neutral exothermic chemistry. They found that exothermic chemistry is the dominant source of heat, but that electron impact excitation of N_2 is a significant heating process above 700 km in daytime. Their detailed calculations of electron-impact excitation of N_2 and CH_4 show that the excitation of N_2 is dominant at altitudes below ~1600 km. In the current study the calculations of the heating produced by electron impact excitation of N_2 were extended to eliminate approximations made by *De La Haye et al.* [2008a].

[3] The mechanism described by *De La Haye et al.* [2008a] was that the impact of photoelectrons and magnetospheric electrons produces vibrational and electronic excitation of N_2. The electronic states radiatively decay (either directly, or via a cascade through one or more intermediate states) to vibrational levels of the ground state. It was assumed that all vibrational energy is "quenched" in collisions and so goes to heat in the atmosphere. For the electronic states, De La Haye et al. calculated a heat fraction, that being the percentage of the electronic state excitation energy that is transferred to a vibrational level of the ground state and hence to the atmosphere. In their calculation only the most probable excitation and decay paths were included. This eliminated four of the electronic states from consideration, as it gave a zero heat fraction. Other approximations were that all molecules excited to vibrational levels of the ground state were in the first vibrational level and that quenching of excited electronic states was negligible.

[4] In the current study, the calculations of the heating rates due to electron-impact excitation of N_2 were extended to eliminate the approximations made by *De La Haye et al.* [2008a]. Initially the previous calculations were repeated to verify that the input data and methods of calculation are correct in the current implementation. They were then repeated for individual (rather than composite) electron-impact cross sections for vibrational excitation, and for updated cross sections for electronic excitation.

[5] The previous calculations were then emulated using a statistical equilibrium method [*Cartwright*, 1978] to verify that the latter is applicable. The statistical equilibrium calculation was then applied to include most excitation, predissociation, radiative, and quenching transitions, rather than the small subset used in the previous work.

2. Reproduction of Previous Results

[6] Aside from verifying that there were no mistakes in the current calculations, a reproduction of the previous calculations was conducted to resolve queries about the energy levels used and to ensure that an adequate electron-flux model was constructed for the current calculations.

[7] In the previous calculations [*De La Haye et al.*, 2008a] the energies of the vibrational levels in N_2 were determined using a standard formula to give E_ν for $\nu = 0, 1, 2\ldots$. This

[1]ARC Centre for Antimatter-Matter Studies, School of Chemical and Physical Sciences, Flinders University, Adelaide, South Australia, Australia.
[2]Department of Physics, Sophia University, Tokyo, Japan.
[3]School of Chemical and Physical Sciences, Flinders University, Adelaide, South Australia, Australia.

0148-0227/10/2010JA015482

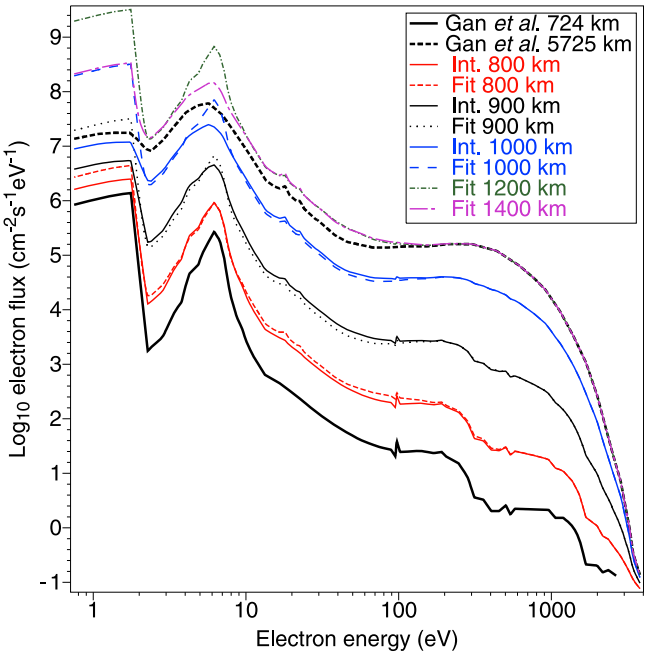

Figure 1. Electron fluxes as a function of electron energy: source spectra [*Gan et al.*, 1992] for 724 km (bold curve) and 5725 km (bold dashed curve), interpolations at 800, 900, and 1000 km (thin curve) and the fitted spectra for 800 km (dashed curve), 900 km (dotted curve), 1000 km (long-dashed curve), 1200 km (dash-dotted curve), and 1400 km (long-dash-dotted curve).

was then applied to determine that quenching of levels $\nu = 6$ and 9 releases 1.826 eV and 2.618 eV as heat in the atmosphere. As the energy released is $E_\nu - E_0$, these energies should be 1.680 eV and 2.472 eV, and thus it seems that the zero point energy $E_0 = 0.146$ eV was not subtracted. This would be a significant error if applied for the first vibrational level, where quenching of the $\nu' = 1$ level would be ascribed an energy of 0.435 eV instead of 0.289 eV. Thus a precise emulation of the previous work was required to determine which energies were used.

[8] The previous work made use of a model of *Gan et al.* [1992] for the electron flux. In this model, energetic electrons are produced by processes in the magnetosphere of Saturn and in photoionization by solar photons in the atmosphere of Titan. These electrons then produce further ionization and secondary electrons. The secondary electrons lose energy in ionization, excitation, and other processes. As the secondary electrons can travel large vertical distances between interactions, the model considers electron transport. The output of the model is presented as a spectrum of electron flux as a function of electron energy at various heights. With decreasing height there is a transfer of electron flux from higher- to lower-energy electrons. The current calculations were limited to the flux spectra produced by this model for 724 and 5725 km [from *Gan et al.*, 1992, Figure 10b]. The shapes and magnitudes of the electron flux spectrum were interpolated for altitudes in between, then adjusted so that the calculated heating rates agreed with those in the previous work. However, it was important to verify that agreement was obtained at 724 and 5275 km without any adjustment, to confirm the validity of the methods of calculation and to determine which energies were used.

[9] The bold curves in Figure 1 show the inward electron flux spectra (cm^{-2} s^{-1} eV^{-1} sr^{-1}) digitized from *Gan et al.* [1992, Figure 10b] and multiplied by 4π. $G_n(E)$ is used here to represent the spectrum labeled n in Figure 1, so $G_2(E)$ and $G_3(E)$ represent the inward electron fluxes at electron energy E at altitudes of 5725 km and 724 km, respectively. A simple model for the isotropic flux $F_s(h, E)$ (cm^{-2} s^{-1} eV^{-1}) at height h (km) is here defined by assuming that the inward flux at 2000 km is the same as at 5725 km, that the inward and outward fluxes are identical below 2000 km, that the fluxes are the same between 1050 km and 2000 km, and that between 760 km and 1050 km the flux at each energy changes logarithmically, i.e.,

$$F_s(h,E) = 4\pi G_2(E) \quad (h > 1050\text{km}), \tag{1}$$

$$F_s(h,E) = 4\pi 10^{\left(\log G_3(E) + \frac{h-724}{1050-724}(\log G_2(E) - \log G_3(E))\right)} \quad (760 < h < 1050\text{km}). \tag{2}$$

These interpolated flux spectra, illustrated by thin solid curves in Figure 1, were multiplied by the integral cross sections used by *De La Haye et al.* [2008a], digitized from their Figure 2, and the N_2 density from the T_A case of *De La Haye et al.* [2008b, Figure 16], scaled to 10^{13} molecules/cm^3 at 600 km to match the value quoted by *De La Haye et al.*

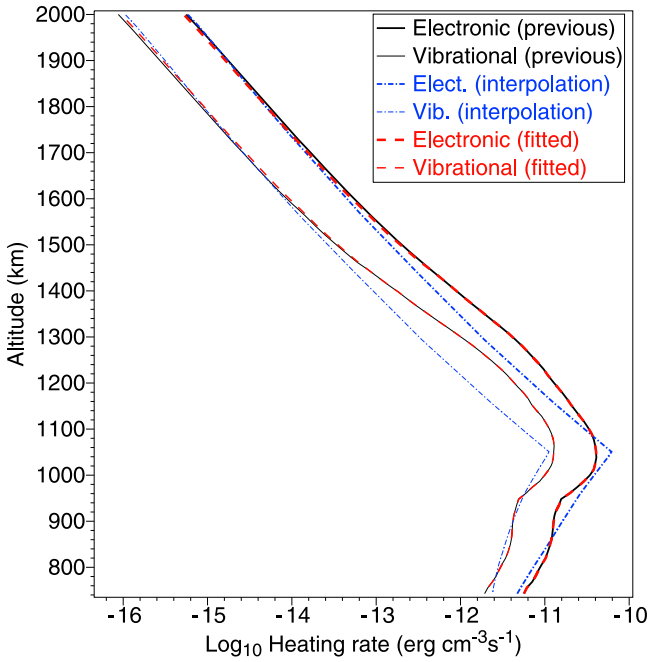

Figure 2. Heating rates (erg cm^{-3} s^{-1}) versus altitude (km) for the previous calculation [*De La Haye et al.*, 2008a] (due to electronic (bold curve) and vibrational (thin curve) excitation), for the interpolated electron fluxes (due to electronic (bold dash-dotted curve) and vibrational (thin dash-dotted curve) excitation), and for the fitted electron fluxes (for electronic (bold dashed curve) and vibrational (thin dashed curve) excitation).

[2008a], to calculate the rates for vibrational and electronic excitation. Their approximation for the vibrational levels, of using cross sections for the sum of all vibrational levels but assuming the excitation is only to level $\nu' = 1$, was followed. The heating rate was then calculated using their assumptions that all molecules in excited electronic states decay to levels of the ground state (without any fraction being quenched in collisions) and that all energy in vibrational levels of the ground state is then transferred to thermal energy of the atmosphere. The heat fraction (energy of the final ground levels divided by energy of the excited state) for each electronic state was taken from *De La Haye et al.* [2008a, Table 2] and multiplied by the excitation rate and the excited-state threshold energy to determine the heating rate. The calculated heating rates are plotted in Figure 2, along with the original values digitized from *De La Haye et al.* [2008a, Figure 4]. (Note that the rates for photoelectrons and magnetospheric electrons have been added up, as the published electron flux spectra [*Gan et al.*, 1992] are for the sum of the two electron sources.)

[10] As expected, the shape of the profile with height in the current calculation is unphysical, as the interpolated flux spectra used here do not embody the complex interactions of the full model [*Gan et al.*, 1992]. However, the good agreement (of both the absolute values and of the ratio of the excited-state to vibrational heating rates) at high and low altitudes, where the electron flux is expected to be close to the available values of *Gan et al.* [1992], suggests that the current implementation of the calculation is correct. As the current calculation used the $\nu = 1 \rightarrow 0$ energy of 0.289 eV, it also confirms that this value must have been used by *De La Haye et al.* [2008a], contrary to the higher values quoted for the $\nu = 6 \rightarrow 0$ and $\nu = 9 \rightarrow 0$ transitions.

[11] Having confirmed that in reproducing the original results the only unknown is the electron flux spectra at the intermediate altitudes, the flux spectra were adjusted so that the calculated heating rates matched those of *De La Haye et al.* [2008a]. This adjustment has two steps: (1) producing a composite spectrum of $G_2(E)$ and $G_3(E)$ so as to match the ratio of calculated electronic state heating rate to vibrational heating rate, then (2) multiplying the spectrum by a factor $S(h)$ required to match the absolute values of the heating rates at height h. The composite spectrum $F_c(h, E)$ is defined by

$$F_c(h,E) = 4\pi S(h)\left(f(h)G_2(E) + (1-f(h))\frac{G_2(6.2)}{G_3(6.2)}G_3(E)\right), \quad (3)$$

where the factor $G_2(6.2)/G_3(6.2)$ scales the two different original spectra to the same value at the peak at 6.2 eV in G_3 and $f(h)$ is the fraction of $G_2(E)$ contributing to the shape of the composite spectrum at altitude h. The ratio of electronic state to vibrational heating rates was calculated using $F_c(h, E)$ with varying $f(h)$ to find the value of $f(h)$ that gives the ratio in the original calculations of *De La Haye et al.* [2008a]. The composite spectrum was then combined with the interpolated spectrum at higher energies to give an adjusted flux spectrum F_a

$$F_a(h,E) = r(h,E)F_c(h,E) + (1 - r(h,E))F_s(h,E), \quad (4)$$

where the factor $r(h, E)$ is

$$r(h,E) = 1 - \frac{1}{\exp\left((E_m/E)^3\right)} \quad (5)$$

and E_m is the energy where the flux is a minimum in the range 30–200 eV. (The function $r(h, E)$ is designed to produce a sharp but smooth transition from the fitted flux spectrum to the interpolated flux spectrum in the region where the spectrum is almost flat.)

[12] Examples of the adjusted flux spectra are shown by dotted/dashed curves in Figure 1, and the resultant heating rates are shown by dashed curves in Figure 2. At altitudes below 1440 km the previous heating rates can be reproduced exactly, with a discrepancy of up to only ~11% at higher altitudes. While it is to be expected that there will be differences between F_a and the fluxes used by De La Haye et al., the adjusted flux is expected to be adequate for the remainder of this study, which is a comparison of the results for different sets of cross sections and transitions.

3. Sensitivity to Electron-Impact Cross Sections

[13] Having verified that the results of *De La Haye et al.* [2008a] can be reproduced, the same calculation was then applied with more recent electron-impact excitation cross sections. It should be noted that as the model of *Gan et al.* [1992] includes the excitation of N_2 in its calculation of the modification of the electron flux spectrum with height, a self-consistent model needs a different flux spectrum to be calculated using the new cross sections. However, this would introduce uncertainty as to which differences are due to using different cross sections and which are due to the effect on the flux distribution of changing the cross sections. Thus the same electron flux is used here so that the relative importance of the cross sections can be assessed.

[14] To calculate vibrational excitation, *De La Haye et al.* [2008a] used an analytical expression that gives the sum of the cross sections for electron-impact excitation of all vibrational levels. They then used the approximation that all vibrationally excited molecules were in the first level to calculate the energy transferred in quenching. The current work uses more recent excitation cross sections for levels $\nu' = 1$–10 [*Campbell et al.*, 2004]. The sum of these is shown in Figure 3, along with the $\nu' = 1$ case, showing that the current cross sections are larger than those used by *De La Haye et al.* [2008a]. In Figure 4 the heating rates calculated with the updated cross sections are shown relative to those calculated using the cross sections of *De La Haye et al.* [2008a]. The current results are calculated for excitation of $\nu' = 1$ only, for excitation of all 10 levels but assigning energy E_1 to all of them, and for all 10 levels with the correct energies. These three cases give heating rates that are progressively larger than the previous values, as expected by examination of the cross sections.

[15] In Figure 3, more recent determinations [*Brunger et al.*, 2003] of the electronic state electron-impact cross sections are plotted for the four states which *De La Haye et al.* [2008a] determined to be significant. The heating rates calculated using these more recent cross sections are shown in Figure 4 by a thin dash-dotted curve. It can be seen they are slightly smaller than those calculated using the original

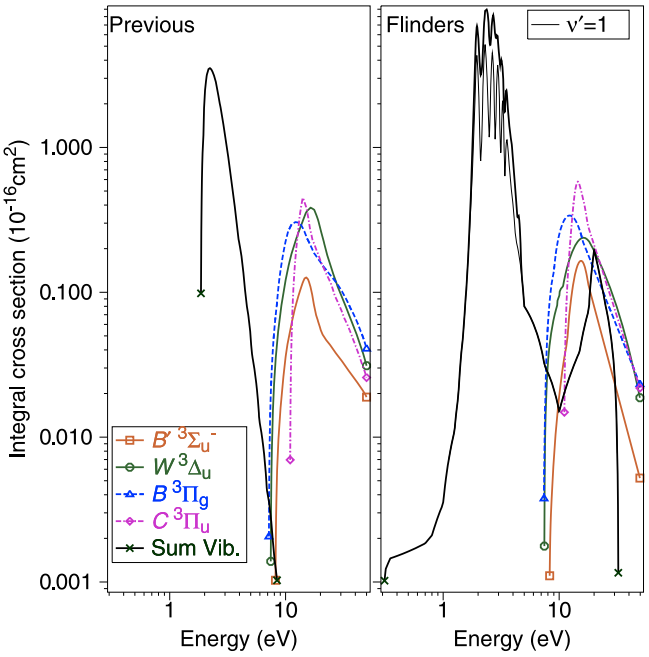

Figure 3. Integral cross sections (10^{-16} cm^2) for electron-impact excitation used (left) in the previous work [*De La Haye et al.*, 2008a] and (right) from Flinders University for the four excited states $B'^3\Sigma_u^-$ (square-curve-square), $W^3\Delta_u$ (circle-curve-circle), $B^3\Pi_g$ (triangle-dashed curve-triangle), and $C^3\Pi_u$ (diamond-dash-dotted curve-diamond) and for the sum of vibrational levels of the ground state (cross-curve-cross). The ICSs for the $\nu' = 1$ level are shown for the Flinders case (thin curve).

cross sections. Examination of Figure 3 shows that the recent cross sections for the $W^3\Delta_u$ state are smaller than those used by *De La Haye et al.* [2008a], while those for the $C^3\Pi_u$ state are larger. Thus the insensitivity of the magnitude of the heating rates to the cross-section set is to be expected. This is verified in Figure 5, where the heating rates due to individual electronic states are shown for the previous and current sets. The values are seen to be very similar for the $B^3\Pi_g$ and $B'^3\Sigma_u^-$ states, while being larger or smaller for the other two states as described above, leading to the result that the overall heating rate is almost the same for the previous and present cross-section sets for the four relevant electronic states.

4. Statistical Equilibrium Calculations

[16] The statistical equilibrium method [*Cartwright*, 1978; *Campbell et al.*, 2006] iteratively solves the continuity equation (by calculating a new value of the population of an energy level that sets the loss rate equal to the gain rate) for each excited level until an equilibrium solution is achieved in which the calculated populations of all levels of all states do not change. The gain for each level includes electron-impact excitation and radiative decay into the level, while the loss includes radiative decay from the level and quenching, in which all energy of the level is lost in a collision leaving the molecule in its ground state. Note that this calculation was not applied to the interaction between the impacting electrons and the molecules, which are not in equilibrium. It was applied here only to determine the redistribution, via the many pathways of predissociation, radiative decay, and quenching, of the energy after excitation. It is an iterative procedure which is applied until a mathematical equilibrium is reached.

[17] *De La Haye et al.* [2008a] included only the most probable excitation for each electronic state and only the one or two most likely radiative transitions from each electronic state. The statistical equilibrium calculation allows all excitations and subsequent transitions (such as predissociation, radiative decay and quenching) to be included in the calculation. Initially it was confirmed that the statistical equilibrium approach is appropriate to the calculation, and correctly implemented. This was done by taking the code for the full calculation and modifying it so that only the excitations and radiative transitions considered by *De La Haye et al.* [2008a] were included.

[18] In Figure 6 the subset of most probable excitations and transitions included by *De La Haye et al.* [2008a] (Figure 6, bottom) can be compared with the larger set used in the current calculation (Figure 6, top). In Figure 6 excitations are represented by up-triangles (open for levels which predissociate, solid for those which do not) plotted at the excitation energy (vertical axis) against the excitation probability (horizontal axis). In Figure 6 (bottom) there is one up-triangle for the ground state and for each excited state, as ascribed by De La Haye *et al.*, while in Figure 6 (top) there is a curve of up-triangles for each excited state,

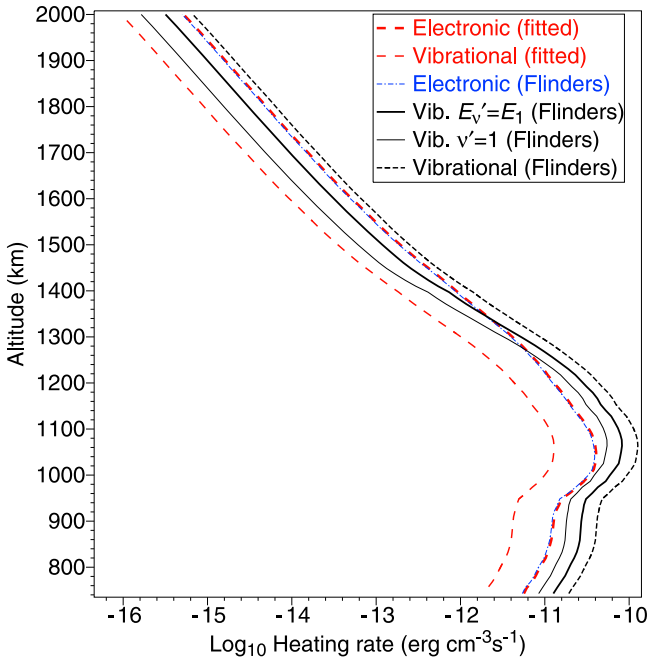

Figure 4. Heating rates (erg cm^{-3} s^{-1}) versus altitude (km) calculated using the previous ICSs [*De La Haye et al.*, 2008a] (for electronic (bold dashed curve) and vibrational (thin dashed curve) excitation) and using the Flinders ICSs [*Brunger et al.*, 2003] for electronic (dash-dotted curve) and vibrational ($\nu' = 1$ only (thin curve), $\nu' = 1$–10 assuming $E_{\nu}' = E_1$ (bold curve) and $\nu' = 1$–10 with correct energies (dashed curve)) excitation.

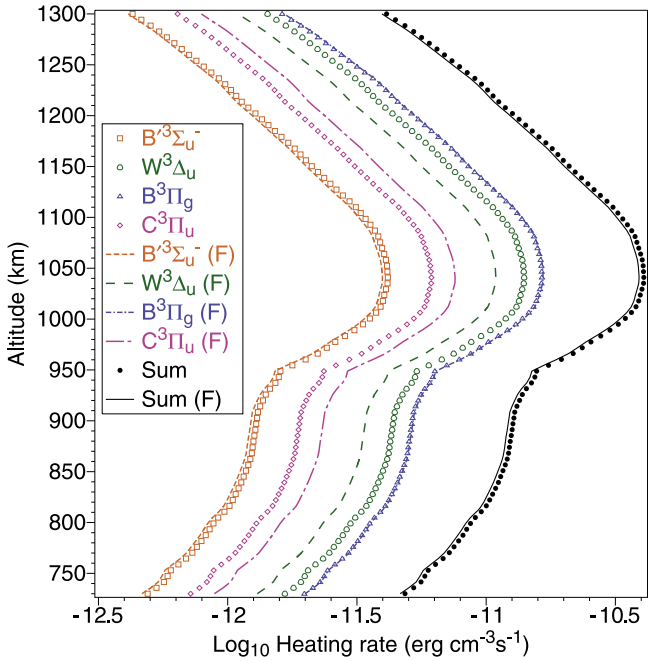

Figure 5. Heating rates (erg cm^{-3} s^{-1}) versus altitude (km) calculated using the previous ICSs [*De La Haye et al.*, 2008a] for excitation of the $B'^3\Sigma_u^-$ (squares), $W^3\Delta_u$ (circles), $B^3\Pi_g$ (triangles), and $C\,^3\Pi_u$ (diamonds) states, and for the Flinders ICSs [*Brunger et al.*, 2003] for excitation of the same states: $B'^3\Sigma_u^-$ (short-dashed curve), $W^3\Delta_u$ (dashed curve), $B\,^3\Pi_g$ (short-dash-dotted curve), and $C^3\Pi_u$(long-dash-dotted curve). Sums of the heating rates for the four previous ICSs (solid circles) and for the four Flinders ICSs (thin solid curve).

showing the distribution as determined by Franck Condon factors, and 10 up-triangles showing the individual excitation rates for levels of the ground state. Radiative transitions are represented by curves or arrows drawn from the initial energy to the final energy of the transition, against the transition probability on the horizontal axis. Quenching rates to the ground level for excited states and to the next vibrational level for excited levels of the ground state are shown by down-triangles plotted at the energy of the quenched level. It is assumed here that in quenching the electronically excited molecule goes to the ground state and all the excitation energy is converted to heat. This does not consider transfer of energy between different excited states and vibrational redistribution within states [*Morrill and Benesch*, 1996; *Kirillov*, 2010]. It needs to be stated that Figure 6 is for 1000 km, because, as excitation probabilities depend on the electron flux spectrum and quenching probabilities on the density of quenching molecules, these probabilities are altitude dependent. (Note that the electronic and vibrational energies in Figure 6 (bottom) are the values used by *De La Haye et al.* [2008a], but the energies for individual levels of the electronic states, rather than the threshold energies, are used to plot the electronic state transitions. This gives an accurate representation of the radiative transitions, while plotting the energies used by De La Haye et al.)

[19] The energy levels and radiative transition probabilities for the electronic states were obtained from *Gilmore et al.* [1992] (the same source as used mainly by *De La Haye et al.* [2008a]). The rates for quenching of excited states by other N_2 molecules were obtained from *Cartwright* [1978]. These are for temperatures of around 500 K in the Earth's atmosphere and so will be overestimates when applied at ~156 K [*De La Haye et al.*, 2008b] in the atmosphere of Titan. Quenching of excited states by methane molecules was not included, as the density of methane is only about 2% of that of N_2 at altitudes below 1000 km [*De La Haye et al.*, 2008b]. Quenching of vibrational levels was performed by using the rates for stepwise vibrational-translational (VT) transitions developed by *Kirillov* [1998] for N_2–N_2 interactions. For quenching of vibrationally excited N_2 by methane, the rate coefficient of 3×10^{-16} cm^3 $molecule^{-2}$ s^{-1} for vibrational-vibrational quenching of methane by N_2 [*Siddles et al.*, 1994] was assumed for VT quenching of N_2 by methane, with the same functional dependence on vibrational level as is given by Kirillov's theory for N_2–N_2. These quenching rates are very low, so the sum was multiplied by 1000 to emulate the assumption of De La Haye et al. that all vibrationally excited molecules are quenched at the altitude of excitation. The radiative

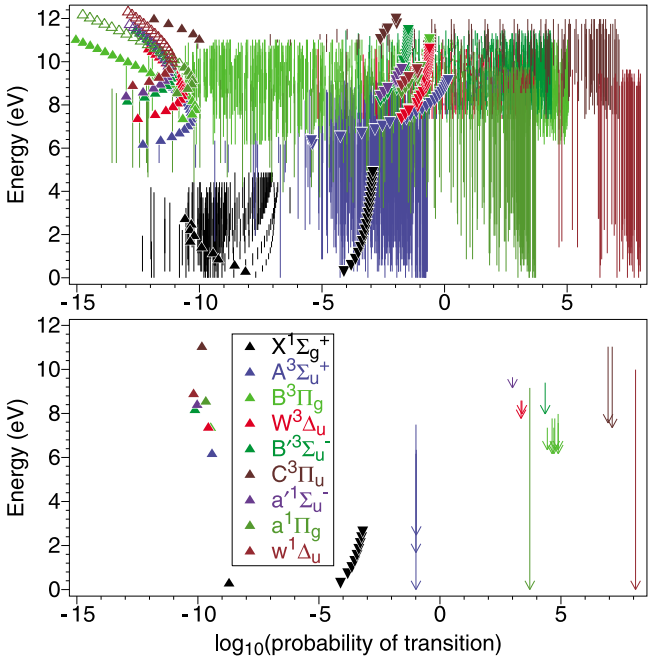

Figure 6. Probabilities of excitations, transitions, and quenching at 1000 km in (bottom) the previous [*De La Haye et al.*, 2008a] and (top) current calculations. Excitations (solid triangles) and predissociations (open triangles) are plotted against probabilities at the excited level energies, while quenching probabilities (solid down-triangles) are plotted at the initial energies. Radiative transitions are shown by lines from the upper to the lower energies, with arrow heads added in the bottom. Symbols and lines for different states are shaded according to the shading of the state names in the legend, while transitions between vibrational levels of the ground state are shown in black.

Table 1. Radiative Transition Probabilities (10^{-9} s^{-1}) for Ground State Transitions ($\nu' \rightarrow \nu''$)

	$\nu'1$	2	3	4	5	6	7	8	9	10	11	12
ν''												
0	19.75	2.52	0.28	0.22	0.15	0.00	0.22	0.17	0.02	0.36	0.23	0.03
1		37.29	7.68	1.09	0.47	0.22	0.00	0.16	0.19	0.00	0.12	0.17
2			52.74	14.84	2.44	0.91	0.44	0.02	0.20	0.45	0.10	0.09
3				66.13	23.70	4.51	1.57	0.65	0.03	0.23	0.57	0.20
4					77.61	33.88	7.19	2.35	0.93	0.09	0.19	0.74
5						87.29	44.91	10.53	3.41	1.30	0.15	0.20
6							95.33	56.70	14.51	4.66	1.69	0.21
7								101.80	68.85	19.02	6.11	2.20
8									106.88	81.07	24.11	7.81
9										110.41	93.36	29.70
10											113.26	105.34
11												114.67

transition probabilities (s^{-1}) for the vibrational levels of the ground state were calculated using [*Jones et al.*, 2006]

$$A_{ji} = \frac{1.680 \times 10^{18} S_{ji}}{\lambda^5 \overline{\omega}}, \tag{6}$$

where λ is the wavelength (Å), $\overline{\omega}$ is the statistical weight and S_{ji} is the line strength. Here,

$$S_{ji} = Q_{ji}^2, \tag{7}$$

where Q_{ji} is the change in electric quadrupole moment (in ea_0^2) during the transition $j \rightarrow i$. The values of Q were obtained from *Cartwright and Dunning* [1974]. Values of A_{ji} are shown in Table 1 for j = 1–12.

[20] The heating rates were determined by extracting quenching rates from the output of the statistical equilibrium program and multiplying by the appropriate transition energy. To separate the vibrational and electronic state contributions to the vibrational quenching, the program was run with just vibrational excitation (where obviously the vibrational quenching is all due to vibrational excitation) and then again with both vibrational and electronic excitation. The heating due to electronic excitation is then found by subtracting the vibrational-only result from that for the total.

[21] In the analysis of *De La Haye et al.* [2008a] it was assumed that all vibrationally excited molecules were quenched somehow. This was emulated in the statistical equilibrium calculation by deactivating radiative transitions and using the same quenching rates as in the full model. The quenching probability for excited states was set to zero to emulate the assumption in the earlier work. The heating rates resulting from this are shown by solid symbols in Figure 7, along with the original results shown by curves. The agreement of these two shows that the statistical equilibrium calculation is implemented correctly. We note that there are smaller heating rates for vibrational excitation at higher altitudes but that this is due to the loss of energy to superelastic electron collisions in the current model. In Table 2 the heat fractions from this analysis are compared with the values of *De La Haye et al.* [2008a], for two emulated cases. The first used the incorrect energies for ν' = 6 and 9 of the ground electronic state, producing heat fractions that are almost the same as in the earlier work. The second used the correct energies, with the result that the heat fractions are substantially less.

[22] The full statistical equilibrium calculation, using the full set of processes as illustrated in Figure 6 (top), gives the heating rates shown by the open symbols. Dots show the heating rates calculated when E_1 = 0.289 eV is assigned as the energy of all vibrational levels. For vibrational excitation, the results are very close to those in Figure 4, except at altitudes above 1700 km, where the current heating rates decline more quickly with increasing altitude than those of De La Haye et al. This is explained by the inclusion in the

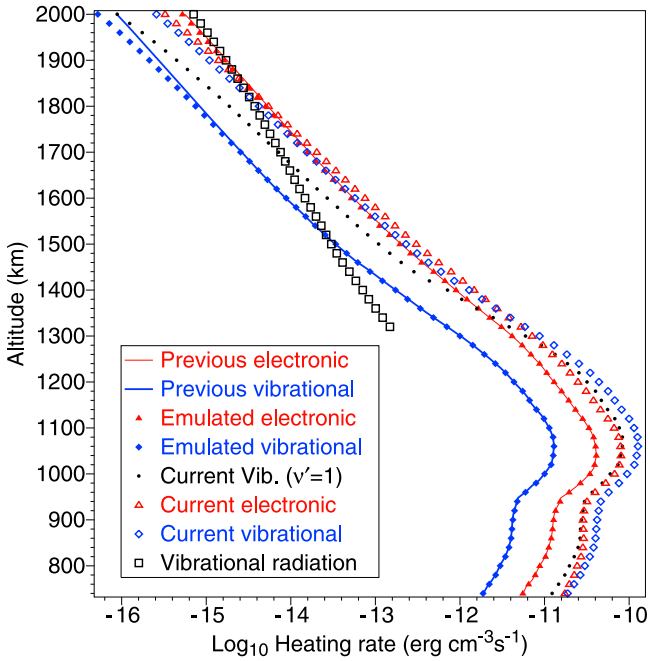

Figure 7. Heating rates (erg cm^{-3} s^{-1}) versus altitude (km) for the previous calculation [*De La Haye et al.*, 2008a] (due to electronic (thin curve) and vibrational (bold curve) excitation), for the emulation of the previous calculations using statistical equilibrium (electronic (solid triangles) and vibrational (solid diamonds)) and the current calculation (vibrational (ν' = 1) (solid dots), electronic (open triangles) and vibrational (open diamonds)). The rate of energy loss due to ground state radiation is also plotted (open squares).

Table 2. Heat Fractions (%) From Previous Work and From Statistical-Equilibrium Calculations

	Previous	Statistical Equilibrium Calculations					
		Emulation		Current Model			
Correct energies		no	yes				
Predissociation		no	no	no	yes	yes	yes
Height (km)		1000	1000	1000	1000	800	2000
$A^3\Sigma_u^+$	0.0	0.0	0.0	35.1	35.1	63.0	11.5
$B^3\Pi_g$	30.9	30.9	27.3	32.9	32.9	35.8	11.7
$W^3\Delta_u$	33.3	33.3	26.9	30.1	30.1	33.3	10.7
$B'^3\Sigma_u^-$	32.1	32.1	26.3	28.3	28.3	32.3	10.0
$a'^1\Sigma_u^-$	0.0	0.0	0.0	13.0	5.2	5.3	2.5
$a^1\Pi_g$	0.0	0.0	0.0	13.9	11.6	11.7	4.8
$w^1\Delta_u$	0.0	0.0	0.0	8.4	1.9	1.9	0.7
$C^3\Pi_u$	18.1	18.1	16.7	20.8	20.8	21.4	7.6
All eight states		15.7	13.2	26.1	25.1	34.6	8.6

current model of ground state radiative transitions, which remove energy at the rate shown by the squares in Figure 7.

[23] The heating rates for the electronic states calculated using statistical equilibrium are substantially higher than those in Figure 4. To investigate where the extra heating arises, the individual contributions for the $B'^3\Sigma_u^-$, $W^3\Delta_u$, $B^3\Pi_g$, and $C^3\Pi_u$ states and their sums are shown in Figure 8 for both the previous and current cross sections. The results are very similar to those in Figure 5, showing that inclusion of many more processes makes little difference. Comparison with the previous result of *De La Haye et al.* [2008a] in Figure 8 shows that inclusion of many more processes has made just a slight increase to the heating rates. This increase is larger at lower altitudes, due to the addition of electronic state quenching (shown by the dotted curve) to the heating rate. This is only significant at altitudes below 800 km.

[24] The origin of the additional excited-state heating in Figure 7 is evident in Figure 9, where the heating rates due to the $A^3\Sigma_u^+$, $a'^1\Sigma_u^-$, $a^1\Pi_g$, and $w^1\Delta_u$ states are shown, again for the two sets of cross sections. These states were not included by *De La Haye et al.* [2008a], as their most probable radiative decay paths led directly to $v'' = 0$. However, using the statistical equilibrium calculation allows all other paths to be included, with the result seen in Figure 9 that the sum of the heating rates for these four states is similar to that for the four states included originally. Electronic state quenching is more significant than in Figure 8. This can be ascribed to the $A^3\Sigma_u^+$ state, as its radiative lifetime of ~2.1 s is much longer than the 0.00005 s of the $a^1\Pi_g$ state.

[25] The heat fractions using the full model are shown in Table 2 for 800, 1000, and 2000 km, with the case at 800 km

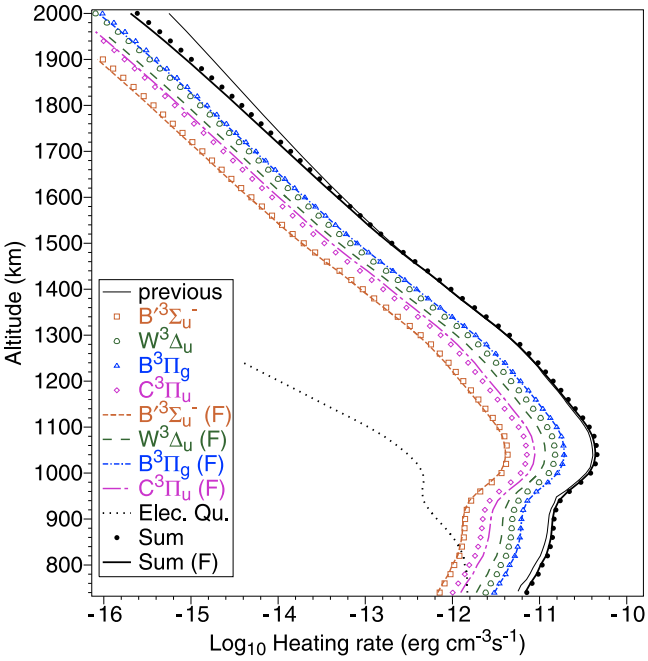

Figure 8. Heating rates (erg cm $^{-3}$ s^{-1}) versus altitude (km) for electronic excitation in the previous work (thin curve) and calculated by statistical equilibrium using the previous ICSs [*De La Haye et al.*, 2008a] for excitation of the $B'^3\Sigma_u^-$ (open squares), $W^3\Delta_u$ (open circles), $B^3\Pi_g$ (open triangles), and $C^3\Pi_u$ (open diamonds) states, and for the Flinders ICSs [*Brunger et al.*, 2003] for excitation of the same states: $B'^3\Sigma_u^-$ (dashed curve), $W^3\Delta_u$(long-dashed curve), $B^3\Pi_g$(dash-dotted curve), and $C^3\Pi_u$(long-dash-dotted curve); for electronic state quenching (dotted curve) for the Flinders case; for all four states plus electronic state quenching for the previous ICSs (solid circles) and for the Flinders ICSs (bold curve).

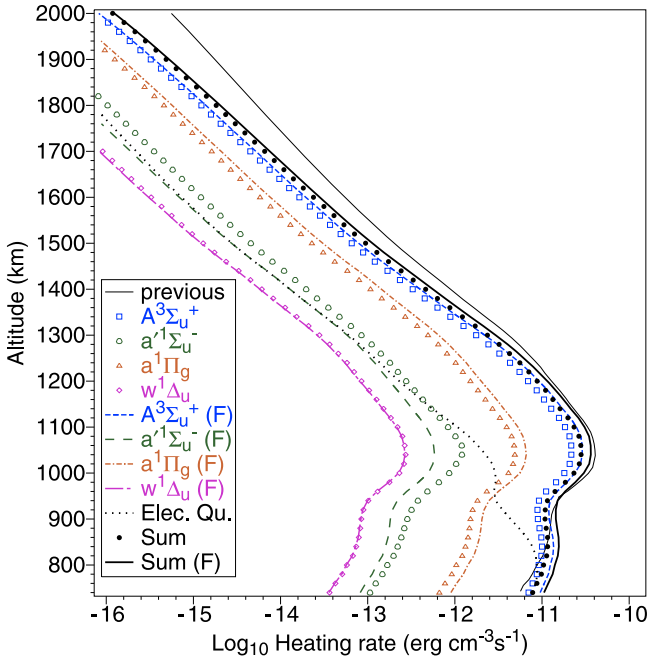

Figure 9. Heating rates (erg cm^{-3} s^{-1}) versus altitude (km) for electronic excitation in the previous work (thin curve) and calculated by statistical equilibrium using the previous ICSs [*De La Haye et al.*, 2008a] for excitation of the $A^3\Sigma_u^+$ (open squares), $a'^1\Sigma_u^-$ (open circles), $a^1\Pi_g$ (open triangles), and $w^1\Delta_u$ (open diamonds) states, and for the Flinders ICSs [*Brunger et al.*, 2003] for excitation of the same states: $A^3\Sigma_u^+$ (dashed curve), $a'^1\Sigma_u^-$ (long-dashed curve), $a^1\Pi_g$ (dash-dotted curve) and $w^1\Delta_u$ (long-dash-dotted curve); for electronic state quenching (dotted curve) for the Flinders case; for all four states plus electronic state quenching for the previous ICSs (solid circles) and for the Flinders ICSs (bold curve).

run with and without predissociation of the singlet states. The values show that the heat fractions for the singlet states are reduced by predissociation, that quenching of $A^3\Sigma_u^+$ is significant at 800 km, and that heat fractions are smaller at 2000 km (due to the heat being lost by radiation). The overall heat fraction for all eight states is also shown. While the earlier work did not give this value, a comparison of the values for the current model with the emulation of the previous work shows a factor of ~2 increase, consistent with the increase seen for the excited-state heating rates in Figure 7.

[26] In the above analysis the quenching rates for ground state vibrational levels were multiplied by 1000 in order to allow a comparison with previous work, in which it was assumed that all vibrationally excited molecules are somehow quenched. Without this arbitrary multiplication, radiation would dominate over quenching down to much lower altitudes than the 1700 km seen in Figure 7. However, both processes would probably be insignificant compared with molecular diffusion [*Kolesnik*, 1982], which would result in ground state excited molecules moving to lower heights before being quenched. This process would need to be considered in a full analysis.

5. Conclusions

[27] Previous calculations of heating rates due to electron-impact excitation of N_2 in the upper atmosphere of Titan have been repeated, using updated cross sections and also using a statistical equilibrium method that allows the populations produced by a large number of competing transitions (excitations, predissociations, radiative transitions, and quenching) to be calculated. It was found that using updated cross sections for excitation of the vibrational levels of the ground state of N_2 gives a significant increase in the heating rates, as does accounting for the energies of all levels rather than assuming that all excitation is in the first vibrational level. It was found that using updated cross sections for the four electronic states that were significant in the previous study makes little difference, with larger cross sections for one state being almost cancelled by smaller cross sections for another. However, the inclusion of more radiative transitions allowed the contribution of four electronic states which were omitted in the previous study to be included, with the finding that these states accounted for about as much heating as the original four. It was found that two of the assumptions in the previous work were justified for most altitudes, i.e., quenching of electronic states and radiation from the vibrational levels of the ground state of nitrogen can be neglected at most altitudes of the study. However, quenching of the $A^3\Sigma_u^+$ state is found to make a significant contribution to the heating rate at altitudes below 900 km, while vibrational radiation is significant above 1700 km. It was also found that for some excited states the use of the most probable excitation and radiative decay pathways is a good approximation for all the processes involved. However, the omission of four states because their most probable excitation and decay pathways led directly to the ground vibrational level of the ground electronic state was shown to be a serious deficiency, as these four states make a similar contribution (to the original four states) through the less probable pathways. Overall it was found that the use of more recent electron-impact excitation cross sections and the inclusion of all excitation, radiative, and quenching pathways led to an increase in the calculated heating rates by a factor of about 2 for electronic state excitation and a factor of about 10 for vibrational excitation. These are thus clearly significant effects.

[28] **Acknowledgments.** This work was supported by the Australian Research Council through its Centers of Excellence Program. H. K acknowledges the Japan Society for the Promotion of Science (JSPS) for his fellowships as grants-in-aid for scientific research and most recently to facilitate his visit to Flinders University. We thank David Cartwright for his generous help with ongoing development of the statistical equilibrium model.

[29] Robert Lysak thanks the reviewers for their assistance in evaluating this paper.

References

Brunger, M. J., S. J. Buckman, and M. T. Elford (2003), Integral cross sections for electron impact excitation of molecules, in *Electron Collisions With Molecules: Scattering and Excitation*, *Landolt-Börnstein*, vol. I/17C, edited by Y. Itikawa, chap. 6.4, pp. 6-132–6-145, Springer, New York.

Campbell, L., M. J. Brunger, D. C. Cartwright, and P. J. O. Teubner (2004), Production of vibrationally excited N_2 by electron impact, *Planet. Space Sci.*, *52*, 815–822.

Campbell, L., D. C. Cartwright, M. J. Brunger, and P. J. O. Teubner (2006), Role of electronic excited N_2 in vibrational excitation of the N_2 ground state at high latitudes, *J. Geophys. Res.*, *111*, A09317, doi:10.1029/2005JA011292.

Cartwright, D. C. (1978), Vibrational populations of the excited states of N_2 under auroral conditions, *J. Geophys. Res.*, *83*(A2), 517–531, doi:10.1029/JA083iA02p00517.

Cartwright, D. C., and T. H. Dunning Jr. (1974), Vibrational matrix elements of the quadrupole moment of N_2 ($X^1\Sigma_g^+$), *J. Phys. B*, *7*, 1776–1781.

De La Haye, V., J. H. Waite Jr., T. E. Cravens, S. W. Bougher, I. P. Robertson, and J. M. Bell (2008a), Heating Titan's upper atmosphere, *J. Geophys. Res.*, *113*, A11314, doi:10.1029/2008JA013078.

De La Haye, V., J. H. Waite Jr., T. E. Cravens, I. P. Robertson, and S. Lebonnois (2008b), Coupled ion and neutral rotating model of Titan's upper atmosphere, *Icarus*, *197*, 110–136.

Gan, L., C. N. Keller, and T. E. Cravens (1992), Electrons in the ionosphere of Titan, *J. Geophys. Res.*, *97*(A8), 12,137–12,151.

Gilmore, F. R., R. R. Laher, and P. J. Espy (1992), Franck-Condon factors, r-centroids, electronic transition moments, and Einstein coefficients for many nitrogen and oxygen band systems, *J. Phys. Chem. Ref. Data*, *21*, 1005–1107.

Jones, D. B., L. Campbell, M. J. Bottema, P. J. O. Teubner, D. C. Cartwright, W. R. Newell, and M. J. Brunger (2006), Electron-driven excitation of O_2 under night-time auroral conditions: Excited state densities and band emissions, *Planet. Space Sci.*, *54*, 45–59.

Kirillov, A. S. (1998), The calculation of TV, VT, VV, VV′ rate coefficients for the collisions of the main atmospheric components, *Ann. Geophys.*, *16*, 838–846.

Kirillov, A. S. (2010), Electronic kinetics of molecular nitrogen and molecular oxygen in high-latitude lower thermosphere and mesosphere, *Ann. Geophys.*, *28*, 181–192.

Kolesnik, A. G. (1982), Vibrational temperature of nitrogen in the ionospheric *F* region (self-consistent calculation), *Geomagn. Aeron.*, *22*, 496–500.

Morrill, J. S., and W. M. Benesch (1996), Auroral N_2 emissions and the effect of collisional processes on N_2 triplet state vibrational populations, *J. Geophys. Res.*, *101*, 261–274.

Siddles, R. M., G. J. Wilson, and C. J. S. M. Simpson (1994), The vibrational deactivation of the bending modes of CD_4 and CH_4 measured down to 90 K, *Chem. Phys.*, *188*, 90–105.

M. D. Bradshaw, School of Chemical and Physical Sciences, Flinders University, P.O. Box 2100, Adelaide, SA 5001, Australia.

M. J. Brunger and L. Campbell, ARC Centre for Antimatter-Matter Studies, School of Chemical and Physical Sciences, Flinders University, P.O. Box 2100, Adelaide, SA 5001, Australia. (laurence.campbell@flinders.edu.au)

H. Kato, Department of Physics, Sophia University, Tokyo, 102-8554, Japan.